THE BORANE ANALOGY: CH LIGAND ORIENTATION IN *arachno*- AND *closo*-BUTTERFLY CLUSTERS

CATHERINE E. HOUSECROFT

Department of Chemistry, University of Notre Dame, Notre Dame, IN 46556 (U.S.A.)

(Received April 24th, 1984)

Summary

The model compound HB_4H_4CH is used as a means of examining the preferred CH ligand orientation when the borane butterfly fragment $HB_4H_4^+$ fragment accommodates CH^- to give either a *closo*- or *arachno*-HB_4H_4CH cluster. The Fenske–Hall quantum chemical technique is used to explore cluster bonding first in terms of carbide protonation and then through the interaction of $HB_4H_4^+$ and CH^-. BH is formally isolobal with $Fe(CO)_3$ and it is shown that the fragment-ligand orbital interactions and mechanism of C–H bond weakening in $HFe_4(CO)_{12}CH$ are modelled successfully using HB_4H_4CH.

Clusters involving metal butterfly units are of interest as models for sites of activation of small molecular units, for example hydrocarbon fragments [1a], and the enhanced reactivity of a μ_4-carbide atom exposed in an M_4 butterfly is significant [1b]. We have previously demonstrated that the tetrairon butterfly $HFe_4(CO)_{12}^+$ has orbital properties that allow it to interact with ligand BH_2^- [2], CH^- [3,4], and CO^{2-} [4], at the same time weakening the internal ligand bonds. The orientation of the ligand with respect to the metal fragment is crucial if the ligand bonds are to be activated. For instance in both $HFe_4(CO)_{12}CH$ [5] and $HFe_4(CO)_{13}^-$ [6] a tilted rather than vertical ligand orientation is exhibited. The structures adopted by these clusters can be rationalized in terms of electron counting rules [7,8] although ambiguities can arise when considering the number of skeletal electrons contributed by the main group ligand [2,9,10]. For a given cluster assignment of *exo*- vs. *endo*-bonding electrons clearly influences the number of designated *cluster* bonding electrons while the *total* number of electrons remained unchanged. Compounds of type $HFe_4(CO)_{12}X$ can be classified as either *closo* or *arachno* depending of whether the ligand X donates 3 or 5 skeletal bonding electrons. The height of X above the Fe_4-butterfly wing–wing axis and the internal dihedral angle of the metal butterfly are two structural parameters that vary sufficiently to allow an observable distinction between a *closo* (ligand = 3 electron donor) or an *arachno* (5 electron donor)

cluster. Ideal *closo* and *arachno* homonuclear skeletons based on the trigonal bipyramid and octahedron repectively are illustrated in Fig. 1. $Fe_4(CO)_{12}C \cdot CO_2CH_3^-$ (a 60 electron unsaturated cluster) and $HFe_4(CO)_{12}CH$ (a 62 electron saturated cluster [9]) are exemplary of these cluster types. In *closo*-$Fe_4(CO)_{12}C \cdot CO_2CH_3^-$, α 130° and the μ_4-C atom lies 0.56 Å above the wingtip axis. (Fig. 2a) [10]. $HFe_4(CO)_{12}CH$ (Fig. 2b) has the ligand C atom lying only 0.06 Å above the tetrairon butterfly wing axis and angle α is 111°. Thus the carbon is considered interstitial within an *arachno* skeleton of four Fe atoms. In addition, note that the tilted CH orientation is consonant with an Fe–H–C bridging interaction and similar ligand bonding modes are evidenced in the *arachno* clusters $HFe_4(CO)_{13}^-$ [6] and $HFe_4(CO)_{12}CH$ [2]. The discussion here centers on $HFe_4(CO)_{12}CH$.

To simplify the calculational procedure, use is made of the "borane analogy" [7b] which allows replacement of a skeletal $Fe(CO)_3$ unit by BH. Thus $HFe_4(CO)_{12}CH$ has an analog HB_4H_4CH. For example in $HFe_4(CO)_{12}CH$, it can be argued that the *arachno* bonding description is merely a steric consequence; viz. the small main group atom "falls" into a cavity between the four metal atoms. Using the isolobal cluster HB_4H_4CH allows an investigation of cluster bonding as a function of cluster atom orbital interactions without the added complication of steric factors. One aim of this paper is to examine to what extent the main group cluster (so far uncharacterized experimentally) can model its transition metal counterpart. In particular, similarities and differences between the bonding capabilities of the $HFe_4(CO)_{12}^+$ and $HB_4H_4^+$ fragments are indicated. The reader should note that the geometry of $HB_4H_4^+$ is chosen to mimic $HFe_4(CO)_{12}^+$ and it is not implied that such a structure would necessarily be adopted by the borane. The simpler AO basis set of the borane

(a)   (b)
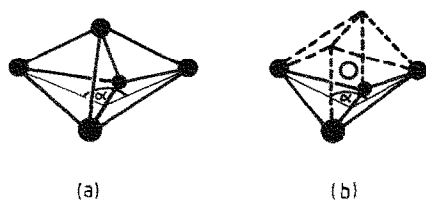
Fig. 1. Idealized homonuclear cluster geometries showing internal dihedral angle, α: (a) *closo*-cluster with α 140° and all cluster atoms in vertex positions; (b) *arachno*-cluster with α 109° and one cluster atom in an interstitial site.

(a)   (b)
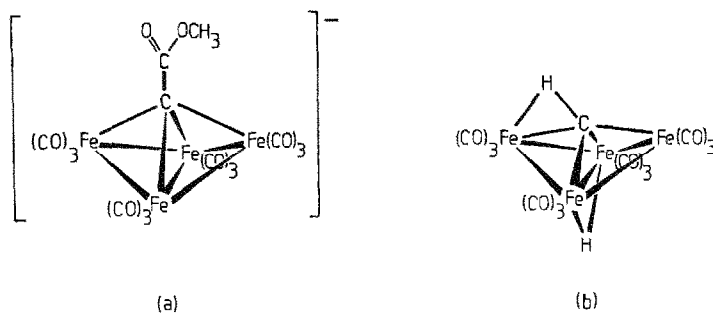
Fig. 2. Structures of (a) $Fe_4(CO)_{12}C \cdot COOCH_3^-$ [9] (*closo*) and (b) $HFe_4(CO)_{12}CH$ (*arachno*) [5].
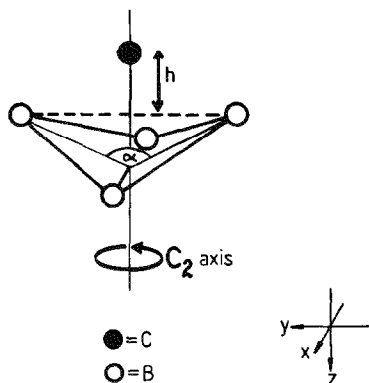
Fig. 3. Schematic representation of the B_4C core of HB_4H_4CH showing the dihedral angle α of the B_4 butterfly, the positioning of the C atom at a height h above the B(wing)–B(wing) axis, and the axis system used throughout this work.

vs. metal fragment allows the examination of orbital changes as a function of skeletal changes (defined in Fig. 3) to be carried out easily. The bonding in HB_4H_4CH is examined both in terms of the protonation of the carbide anion, $HB_4H_4C^-$ and the interaction of $HB_4H_4^+$ with CH^-. The MNDO method of optimizing cluster geometry on an energetic basis has been used to compare the stabilities of protonated borane and carborane clusters [11]. As expected, such results compliment rationalizations made by considering the character of the highest occupied molecular orbitals of the parent non-protonated clusters [11b]. The relatively simple frontier orbital approach is employed here.

Results and discussion

$HB_4H_4C^-$. Geometrical variations pertinent to the structural differences noted in $HFe_4(CO)_{12}X$ or related clusters are applied to $HB_4H_4C^-$ and are summarized in Fig. 3. The *closo*-model (I) has α set at 140° while the *arachno*-model (II) has α 125° [12]. Irrespective of changes in α and h (Fig. 3), the filled MO's of I and II can be categorized simply as BH terminal bonding MO's or B_4C-cluster bonding MO's of σ, π_x, π_y, or δ-symmetry with respect to the C_2 axis of the B_4-butterfly unit. Since the δ-MO has no carbon contribution, it can be ignored when considering carbide protonation. Figure 4 correlates the highest filled MO's of I and II and schematically illustrates MO 10 (σ) in I (second highest filled MO) and MO 11 (π_y) in II (HOMO). Assuming that the empty $1s$ orbital of the incoming proton will interact with the highest available filled MO of the carbide that possesses suitable symmetry, one sees from Fig. 4 that the MO reordering in going from I to II is significant. I should accept H^+ into a σ-orbital located on carbon thus forming a terminal C–H bond, whereas II will be protonated in a B(wing)–C bridging site. Hence, for an *arachno*-cluster with interstitial carbon, the CH ligand adopts a tilted orientation with respect to the borane butterfly while for the *closo*-cluster, the CH is radially oriented with respect to the B_4C cage. The result for II agrees with recent interpretations of the CH geometry in the isolobal complex $HFe_4(CO)_{12}CH$ (Fig. 2b) which has been described in terms of protonating $HFe_4(CO)_{12}C^-$ [13]. It is pleasing that the much simpler borane model mimics the bonding picture for the transition metal

TABLE 1

GEOMETRICAL PARAMETERS FOR THE PROTONATION OF I [a]

h (Å) [b]	0.0	0.2	0 4	0.6	0 8	0.93
B(wing)–C (Å)	1.42	1.44	1.50	1.55	1 63	1.70
B(hinge)–C (Å)	1.02	1.13	1.27	1.42	1.58	1.69

[a] All B–B distances 1.75 Å; B–H$_{terminal}$ 1.19 Å; B–μ-H 1.34 Å Angle α (Fig. 3) 140 °. [b] h = height of C above wing-tip axis, defined in Fig. 3.

system. Moreover, the main group model predicts the expected difference in protonation of an interstitial or vertex carbide.

In going from I to II, two geometrical parameters are varied, α and h (Fig. 3). The question arises: "Which factor controls the protonation site preference: the dihedral angle (α), the position of the C atom (h), or both factors operating together?" To answer this, a series of calculations was performed on I (Table 1) varying h ($0.0 \leqslant h \leqslant 0.93$) but keeping α constant at 140°. Figure 5 correlates the MO's of each model paying attention to changes in MO's 9–11 that are pertinent to the protonation of I. MO's 9–11 have δ, π_y or σ-symmetry, defined with respect to the C_2 axis of I. From Table 1, the unrealistic requirements placed on I when $h \leqslant 0.4$ Å are obvious. Although a true interstitial carbon should lie exactly on the wing–wing axis of the boron butterfly, steric requirements of the cluster cannot be overruled. For I the lowest plausible C position that might still yield an *arachno* skeleton is $0.4 < h < 0.6$ Å (Table 1). Figure 5b indicates that such a structure exhibits a HOMO of π_y symmetry, giving a model that is reminiscent of II with carbide protonation yielding a B(wing)–H–C bridge. So even with α increased from 125° (II) to 140° (I), it appears as though B(wing)–C bridge protonation is attained once the C atom approaches a near interstitial site. Disregarding steric constraints and forcing the
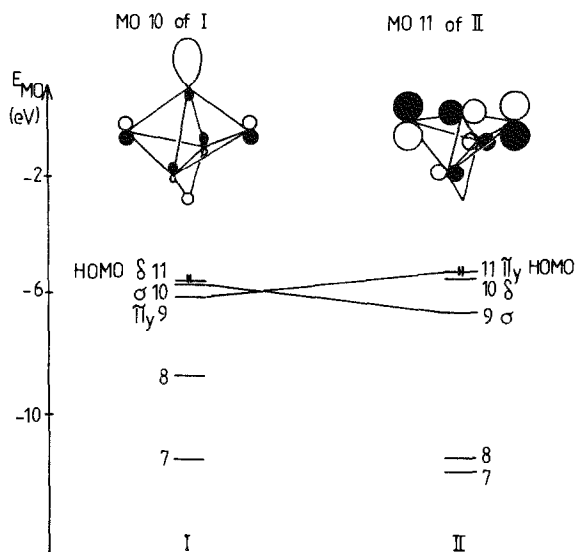
Fig. 4. Correlation of the highest filled MO's of I and II with schematic representations of the MO in each case that will govern site of protonation.

carbon onto the wing–wing axis (h 0.0 Å) in fact yields a HOMO of σ-symmetry (Fig. 5a) but having no optimum site for protonation.

Raising the carbon ($h > 0.6$ Å) stabilizes the π_y-MO (Fig. 5) and reveals a σ-MO (MO 10) as the orbital controlling protonation (Fig. 5c). The extreme model for I with h 0.93 Å is of course identical to II exhibiting a high lying σ-MO with an sp_z hybrid located on carbon. Pulling the carbon out of the cluster produces a striking effect of sequential hybridization. An originally pure p_z orbital on carbon in the HOMO for h 0 Å eventually becomes 79% $2p_z$ and 21% $2s$ in MO 10 when h 0.93 Å and this orbital directionalization enhances terminal C–H bond formation.

The known tetrametal butterfly systems that exhibit tilted ligands (e.g. $HFe_4(CO)_{12}CH$, Fig. 2b) do so with the ligand interacting with a wing-tip rather than hinge metal atom. This can be rationalized in terms of the borane analogy as follows. Protonation of $HB_4H_4C^-$ to give a B(hinge)–H–C interaction requires the incoming proton to approach a site of electron density between B(hinge) and C atoms; i.e. the carbide anion should possess a high lying filled MO of π_x symmetry. Figure 5 shows that although a π_x orbital is destabilized on going from h 0.0 to 0.93 Å, it is always lower in energy than the σ or π_y-MO's. Hence, terminal or B(wing)–C bridge protonation should always be preferred.

Thus, in terms of carbide protonation, the preference for a terminal CH or bridging B–H–C mode of bonding can be rationalized for the *closo-* or *arachno-*
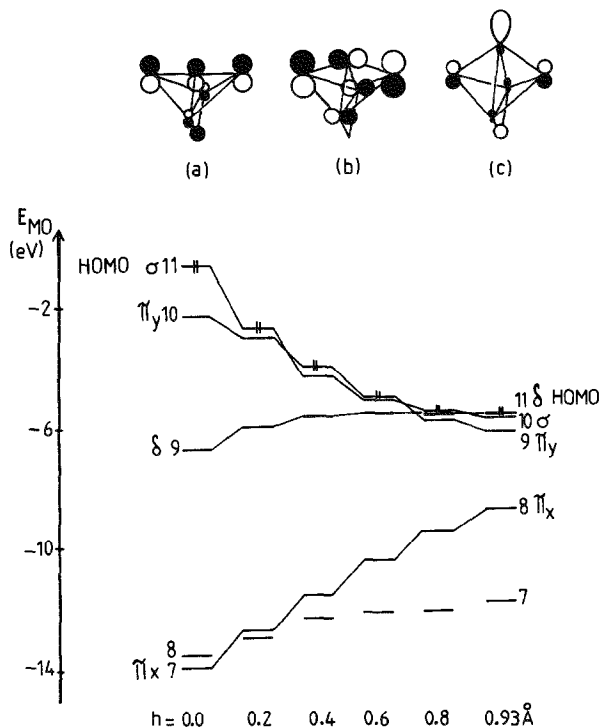
Fig. 5. Correlation diagram indicating changes in MO energies in I as a function of the carbon position defined by the height h (Fig. 3). Schematic representations of those MO's controlling protonation site are shown in (a) for h 0.0 and 0.2 Å, (b) for h 0.4 and 0.6 Å, (c) for h 0.8 and 0.93 Å.

HB_4H_4CH model compounds respectively and the primary controlling factor attributed to the C atom siting. One could argue however that this positioning is a steric consequence of a change in the B_4-butterfly dihedral angle and therefore the two factors are not completely separable.

$HB_4H_4{}^+$. As we have previously used the Fenske–Hall technique of fragment orbital analysis to delineate the interaction of the $HFe_4(CO)_{12}{}^+$ fragment with the CH^- ligand [3,4], it is logical to examine the interaction of isolobal $HB_4H_4{}^+$ with CH^- to see what similarities exist between the two bonding descriptions. $HFe_4(CO)_{12}CH$ (Fig. 2b) is characterized as an *arachno* cluster with α 111° [5], so initially the interaction of CH^- with a 125° $HB_4H_4{}^+$ [12] is examined with the ligand positioned vertically (IIIb) and in a tilted orientation (IIIa). In addition CH^- interaction with 140° $HB_4H_4{}^+$ (*closo* geometry) is explored; IVa has a tilted and IVb a vertical CH.

SCHEME 1

IIIa   IIIb   IVa   IVb

● = C   ○ = BH   • = H
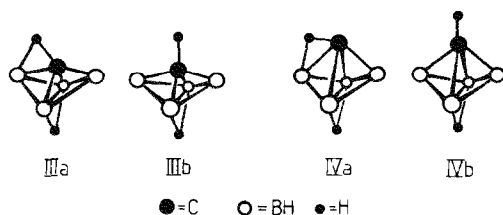
The orbitals of the $HB_4H_4{}^+$ fragment consist of terminal BH bonding orbitals (1–5), high lying antibonding orbitals and a set of "frontier" cluster orbitals (6–11) (Fig. 6). Changing the butterfly angle from 125° to 140° reorders the orbitals (Table 2) and, as expected, small angular perturbations in the fragment orbitals reflect the angular change in the borane skeleton. The orbitals of the two fragments are readily comparable however and the frontier orbitals are easily correlated with those of the isolobal $HFe_4(CO)_{12}{}^+$ fragment (Table 2 and Fig. 6). From a consideration of nodal properties alone, orbital 80 of $HFe_4(CO)_{12}{}^+$ appears to lie at unusually high energy, a consequence of prevalent metal–carbonyl antibonding character [4]. In $HB_4H_4{}^+$, the comparable orbital (6) is the lowest lying "frontier" orbital as anticipated. Note that this transition metal/main group correlation implies that orbitals 12 and 13/14 (125°/140°) of $HB_4H_4{}^+$ will be involved in fragment-ligand interaction. In fact they are high lying and better thought of as fragment antibonding orbitals playing no active role in binding a ligand as evidenced by fragment-ligand Mulliken overlap populations in the $HB_4H_4{}^+/CH^-$ analysis. This actually turns out to parallel the situation for the $HFe_4(CO)_{12}{}^+$ fragment quite nicely; we have indicated previously that orbital 79 (Table 2) is fragment-ligand nonbonding and forms the LUMO in each of $HFe_4(CO)_{12}CH$ [3,4], $HFe_4(CO)_{12}BH_2$ [2], and $HFe_4(CO)_{13}{}^-$ [4], and orbital 81 (δ-symmetry) is transferred unperturbed to an empty MO in each of these complexes. Of the remaining orbitals (6–11) comprising the "frontier" set of the $HB_4H_4{}^+$ fragment, orbital 9 in the 125° butterfly (8 for 140° fragment) is nonbonding with respect to the CH^- ligand by virtue of it possessing δ-symmetry (Fig. 6).

In going from a transition metal to a main group system there is a less well defined segregation of orbital "packages". Figure 6 indicates that for $HFe_4(CO)_{12}{}^+$,

TABLE 2

$HB_4H_4^+$ vs. $HFe_4(CO)_{12}^+$ FRONTIER ORBITALS

Orbital in 125° $HB_4H_4^+$	Orbital in 140° $HB_4H_4^+$	Symmetry	WH [a]	HH [a]	Correlated with orbital in $HFe_4(CO)_{12}^+$ [b]
13 [c]	14 [c]	δ	ab	ab	81
12 [c]	12 [c]	π_x	ab	ab	79
11	10	π_y	nb	nb	78
10	11	σ	ab	b	77 (LUMO)
9 (LUMO)	8 (HOMO)	δ	b	ab	74
8 (HOMO)	9 (LUMO)	π_x	b	ab	76 (HOMO)
7	7	π_y	b	b	75
6	6	σ	b	b	80

[a] WH = Wing-hinge; HH = hinge-hinge; b = bonding; ab = antibonding; nb = nonbonding. [b] See ref. 2.
[c] These orbitals are too high lying to be considered as "frontier" orbitals and do not interact with the ligand as evidenced by fragment-ligand overlap populations (see text).

antibonding, frontier, metal-containing, localized M–μ-H–M and metal–carbonyl orbitals can be distinguished from one another [2–4]. In $HB_4H_4^+$ this is not so. B–μ-H–B bridge character is not localized but contributes to four of the eight filled fragment orbitals. The demarkation between BH bonding and frontier orbitals (5 to
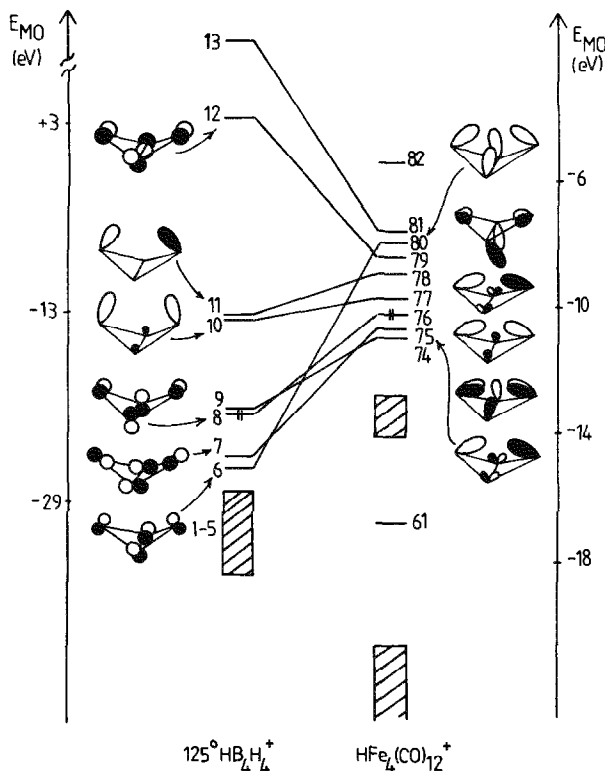
Fig. 6. Correlation of the orbitals of fragments 125° $HB_4H_4^+$ and $HFe_4(CO)_{12}^+$ both of which are derived from *arachno* clusters. The MO energy scale on the left refers to $HB_4H_4^+$ and that on the right to $HFe_4(CO)_{12}^+$.

6) is not obvious from orbital energies. The indistinction between "high lying frontier" and "antibonding" orbitals is also noted. Thus it is not surprising that the following correlation of $HB_4H_4^+$ and CH^- orbitals with those in HB_4H_4CH reveals a far greater degree of fragment orbital mixing than is found in fragment analyses of $HFe_4(CO)_{12}X$ species [2–4].

125°HB₄H₄CH (III): Arachno-model. Summing the filled MO energies [14] of IIIa vs. IIIb (Scheme 1) indicates IIIa to be more stable than IIIb by 3.1 eV. The greatest single contributory factor appears to be the stabilization of MO 2 which in IIIb is a fragment-ligand σ-bonding MO. On going from IIIb to IIIa, σ and π MO's are no longer mutually exclusive (i.e. C_{2v} symmetry is reduced to C_s) and MO 2 mixes in fragment orbitals 7 and 11 (π_y). Figure 7a represents the $(11\text{-}2\sigma)$ interaction that causes stabilization of MO 2; note that the interaction leads to the generation of a B–H–C bridge bond. In IIIb, the HOMO contains a $(7/11\text{-}2\pi)$ interaction and on going to IIIa, this combination picks up 10 (σ) character with a net MO stabilization of 0.5 eV. The newly acquired $(10\text{-}2\pi)$ interaction is represented in Fig. 7b. Fragment-ligand Mulliken overlap populations (Table 3) reinforce the significance of the $(11\text{-}2\sigma)$ and $(10\text{-}2\pi)$ interactions in IIIa. Together these newly allowed interactions account for an overlap gain of 0.303, approximately twice the net overlap gain for fragment orbitals 6–11 with CH^- orbitals in going from IIIb to IIIa. The major competing factor is the marked loss in $(11\text{-}2\pi)$ overlap (Table 3 and Fig. 7c). Other gains and losses in fragment-ligand overlaps are insignificant
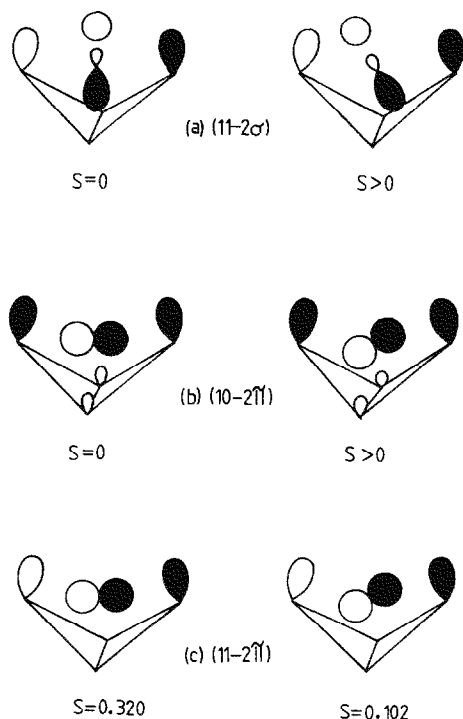
Fig. 7. Important fragment-ligand orbital interactions in IIIa vs. IIIb: (a) and (b) are symmetry disallowed in IIIb but allowed in IIIa. The gain in fragment-ligand Mulliken overlap population, S, indicated qualitatively in (a) and (b) is offset partly by the loss illustrated in (c).

TABLE 3

MULLIKEN OVERLAP POPULATIONS[a] FOR $125°\,HB_4H_4^+/CH^-$

$125°\,B_4H_4^+$ orbital	CH⁻ orbital					Change[b] in overlap per $HB_4H_4^+$ orbital
	1σ	2σ	1π	2π	$3\sigma^\star$	
$11(\pi_y)$	0.000	0.000		0.320	0.000	+0.004
	(0.057)	(0.157)		(0.102)	(0.008)	
$10(\sigma)$	0.066	0.035		0.000		+0.137
	(0.086)	(0.006)		(0.146)		
$8(\pi_x)$			0.345			0.000
			(0.345)			
$7(\pi_y)$		0.000		0.040	0.000	−0.003
		(0.023)		(0.000)	(0.014)	
$6(\sigma)$	−0.029		0.000			+0.015
	(0.000)		(−0.014)			
Change[b] per CH⁻ orbital	+0.106	−0.151	0.000	−0.126	+0.022	Net = +0.153[c]

Net change[b] in overlap for $HB_4H_4^+$ orbitals 1–5 with CH⁻ = −0.080

Total = +0.073

[a] Values without parentheses refer to IIIb; values with parentheses refer to IIIa. [b] Change in going from IIIb to IIIa. [c] The total $HFe_4(CO)_{12}CH$ is +0.031 favoring a tilted CH [4].

compared to the $(11\text{-}2\sigma)/(10\text{-}2\pi)$ vs. $(11\text{-}2\pi)$ competition, (Table 3).

For the CH⁻ ligand itself, the transition from IIIb to IIIa leads to C–H bond weakening as evidenced by the ligand orbital populations listed in Table 4. Both 1σ and 2σ orbitals lose significant electronic charge while the population of the $3\sigma^\star$ orbital increases slightly [15]. The loss of charge from the 2σ orbital is consonant with the acquisition of $(11\text{-}2\sigma)$ in IIIa. Orbital 11 is empty in $HB_4H_4^+$ and can accept charge from the filled CH⁻ 2σ orbital. Though less important than 2σ from a fragment-ligand bonding point of view, the CH⁻ 1σ orbital plays a significant role in C-H bond weakening as noted from Table 4.

Comparison of III with $HFe_4(CO)_{12}CH$. The preference for a tilted over vertical CH⁻ orientation with respect to the $HFe_4(CO)_{12}^+$ fragment is marginal [3,4]. By considering the $HFe_4(CO)_{12}^+$ vs. $HB_4H_4^+$ correlations made in Fig. 6, one can compare the fragment-ligand orbital interactions that are most affected by ligand tilting in $HFe_4(CO)_{12}CH$ and III. In the metal system, the orbital combinations that most strongly favor CH⁻ tilting are $(78\text{-}2\sigma)$ and $(77\text{-}2\pi)$ plus a smaller contribution from $(75\text{-}3\sigma^\star)$ with part of this fragment-ligand overlap gain offset by $(78\text{-}2\pi)$ loss. Figure 6 shows metal vs. borane fragment orbital correlations as follows: 75(filled)-

TABLE 4

CH⁻ ORBITAL POPULATIONS IN III

CH⁻ orbital	1σ	2σ	1π	2π	$3\sigma^\star$
Free CH⁻	2.0	2.0	1.0	1.0	0.0
IIIa	1.570	1.016	0.979	1.128	0.035
IIIb	1.703	1.072	0.951	1.022	0.013

7(filled). 77(empty)-10(empty). 78(empty)-11(empty). A glance at Table 3 and the discussion above reveals that the main group cluster is indeed paralleling the transition metal system quite nicely, although the role of the $(7\text{-}3\sigma^\star)$ interaction in IIIa is overshadowed by the effects of the $(10/11\text{-}2\sigma/2\pi)$ interactions.

One further point remains. The fragment analysis of III shows that $HB_4H_4^+$ orbitals 1–5, formally assigned as BH bonding orbitals, interact quite significantly with those of the ligand. In $HFe_4(CO)_{12}CH$, the metal carbonyl MO's are on the whole, unperturbed M–CO orbitals carried directly accross from the $HFe_4(CO)_{12}^+$ fragment [3,4]. Any M–CO/CH^- orbital interaction is negligible. This difference between metal and main group systems is apparent from fragment-ligand Mulliken overlaps. For the $HFe_4(CO)_{12}^+/CH^-$ interaction, one can rationalize ligand orientation without needing to consider more than the fragment frontier orbitals (Fig. 6). For the $HB_4H_4^+/CH^-$ interaction, Table 3 lists a net overlap gain of 0.153 (fragment orbitals 6–11 only) or 0.073 (fragment orbitals 1–11) on going from IIIb to IIIa. Hence, the result of including the BH bonding orbitals is significant but does not alter the conclusions made earlier.

Thus by using HB_4H_4CH as a model for the bonding in $HFe_4(CO)_{12}CH$ the following points are made: (i) on a qualitative level, major fragment-ligand interactions that control ligand orientation in the metal system can be deduced from the simple main group analog; (ii) causes for C–H bond weakening in $HFe_4(CO)_{12}CH$ are equally apparent in HB_4H_4CH although weakening by loss of charge from the filled ligand σ-orbitals tends to predominate over transfer of charge to the empty C–H antibonding orbital when $Fe(CO)_3$ is replaced by BH; (iii) the inactive role of the metal carbonyl orbitals with respect to ligand binding is not paralleled by BH
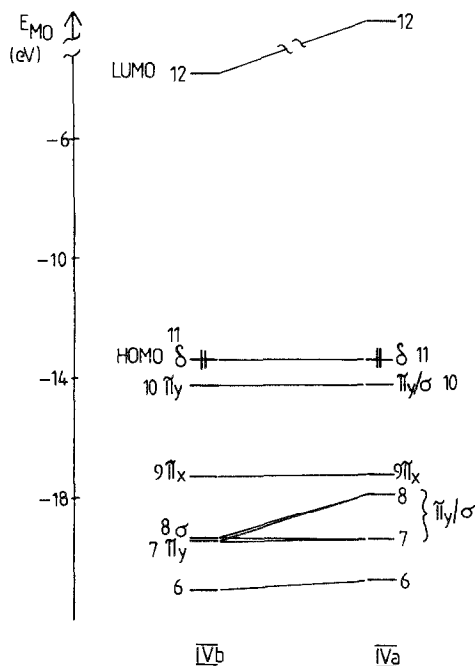
Fig. 8. Correlation diagram for MO's in IVb and IVa.

TABLE 5

MULLIKEN OVERLAP POPULATIONS[a] FOR 140° HB$_4$H$_4^+$/CH$^-$

140° HB$_4$H$_4^+$ orbital	CH$^-$ orbital					Change[b] in overlap per HB$_4$H$_4^+$ orbital
	1σ	2σ	1π	2π	3σ*	
11 (σ)	0.014 (0.080)			0.000 (0.053)		+0.119
10 (π$_y$)	0.000 (0.037)	0.000 (0.208)		0.335 (0.064)		−0.026
9 (π$_x$)			0.307 (0.038)			+0.001
7 (π$_y$)				0.011 (0.000)	0.000 (0.011)	0.000
6 (σ)	−0.038 (−0.010)	0.157 (0 067)		0.000 (0.045)		−0.017
Change[b] in overlap per CH$^-$ orbital	+0.131	+0.118	+0.001	−0.184	+0.011	Net = +0.077
	Net change[b] in overlap for HB$_4$H$_4^+$ orbitals 1–5 with CH$^-$ =					−0.020

[a] Values without parentheses refer to IIIb; value with parentheses refer to IIIa. [b] Change on going from IIIb to IIIa.

bonding orbitals. Ignoring (iii) above implies a more definitive preference for the tilted CH orientation in the borane than the metal cluster (Table 3).

140° HB$_4$H$_4$CH (IV): Closo model. In going from III to IV, the borane butterfly angle is increased by 15° and the C atom of the ligand raised 0.54 Å (Scheme 1). Summing the energies of the filled MO's in IVa vs. IVb indicates a 2.8 eV preference for IVb. The most obvious destabilization effect as the ligand tilts is that suffered by MO's 7 and 8 (Fig. 8) and this is consistent with substantial loss in fragment-ligand overlaps suffered by the interactions present in these MO's, viz. (6-1σ), (7-2π) and (10-2π) (Fig. 9). Net fragment-ligand Mulliken overlap populations are listed in Table 5, emphasis being laid on the fragment "frontier" orbitals 6–11. It is immediately apparent that these values do not reiterate the suggestion made earlier that structure IVb is preferred to IVa. Tilting the ligand leads to significant overlap

(a) (6-1σ)   (b) (7-2π̄)   (c) (10-2π̄)

ΔMOP −0.045   ΔMOP−0.037   ΔMOP−0.032
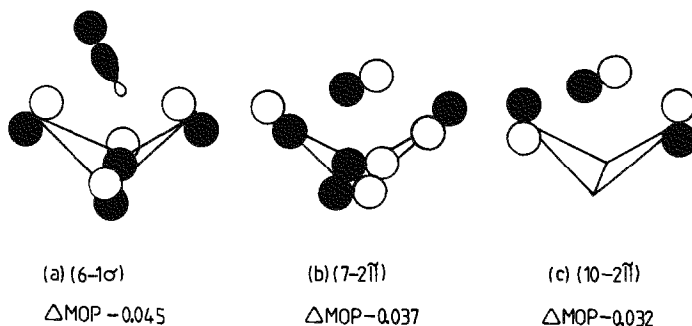
Fig. 9. Schematic representations of fragment-ligand orbital interactions in IVa that contribute to the destabilization of MO's 7 and 8 in going from IVb to IVa. The same interactions are present in IVb. ΔMOP = change in fragment−ligand Mulliken overlap population within MO's 7 and 8 as the CH$^-$ ligand tilts.

gains involving fragment orbital 11, and this contributes to an apparent net preference for a tilted rather than vertical ligand. The inclusion of the BH orbitals (1–5) now becomes crucial. The change in net overlap with CH^- orbitals as the CH is tilted is approximately the same for both the $125°$ and $140°\,HB_4H_4{}^+$ fragments (Table 3 vs. Table 5), but taken against the net frontier orbital-ligand overlap, it is sufficient to tip the balance between IVa and IVb but not between IIIa and IIIb. This would imply that in main group *closo*-clusters *exo*-ligand bonding orbitals are not wholly innocent bystanders when it comes to binding vertex cluster units to the *closo*-cage. This is presumably due to the energies of both the $HB_4H_4{}^+$ *exo*-ligand and frontier orbitals being comparable with those of the vertex ligand orbitals. On the other hand, it is not surprising that interstitially bound ligands interact more prevalently with core cluster orbitals as examplified here by the bonding capability of an open *arachno*-skeleton.

Method

Fenske–Hall calculations [16] were carried out on $HB_4H_4C^-$ (I and II) and on HB_4H_4CH (III and IV). All geometries were idealized with the HB_4H_4C unit having C_{2v} symmetry. I and IV had α $140°$ and in II and III, α $125°$ (Fig. 3). In I, the C atom was placed in a vertex position with h 0.93 Å giving B(wing)–C 1.70 Å and B(hinge)–C 1.69 Å. In II the carbon was as near interstitial as steric requirements would sensibly allow [12] with h 0.39 Å, giving B(wing)–C = B(hinge)–C = 1.40 Å. III and IV are generated from II and I respectively by the addition of a proton to the carbon. All terminal BH were set at 1.19 Å, bridge BH 1.34 Å and CH 1.09 Å. For each of III and IV, two structures were considered. IIIa and IVa had a terminal C–H bond while IIIb and IVb had the proton positioned between the carbon and a wing-boron atom such that B(wing)–H 1.34 Å (Scheme 1). In addition a series of calculations was carried out on I with the C atom at various positions on the boron butterfly C_2 axis (Table 1). The axis system used in each calculation is shown in Fig. 3. Throughout the discussion, "orbitals" refer to molecular orbitals of the fragments and "MO's" to those of the complexes.

The Fenske–Hall calculations employed single-ζ Slater functions for the $1s$ and $2s$ functions of C and B. The exponents were obtained by curve fitting the double-ζ functions of Clementi [17] while maintaining orthogonal functions; the double-ζ functions were used directly for the $2p$ functions. For H, an exponent of 1.16 was used.

Acknowledgements

References

1 (a) See for example: R.M. Gavin, J. Ruett, and E.L. Muetterties, Proc. Natl. Acad. Sci. U.S.A, 78 (1981) 3981; E.L. Muetterties, Chem. Soc. Rev., 83 (1983) 283; M.A. Drezdzon, K.H. Whitmire; A.A. Bhattacharyya, W.-L. Hsu, C.C. Nagel, S.G. Shore, and D.F. Shriver, J. Am. Chem. Soc., 104 (1982) 5630; (b) J.W. Kolis, F. Basolo and D.F. Shriver, J. Am. Chem. Soc., 104 (1982) 5626.

2 T.P. Fehlner, C.E. Housecroft, W.R. Scheidt and K.S. Wong, Organometallics, 2 (1983) 825.

3 C.E. Housecroft and T.P. Fehlner, Organometallics, 2 (1983) 690.

4 T.P. Fehlner and C.E. Housecroft, Organometallics, 3 (1984) 764.

5 M.A. Beno, J.M. Williams, M. Tachikawa, and E.L. Muetterties, J. Am. Chem. Soc., 103 (1981) 1485.

6 M. Manassero, M. Sansoni and G. Longoni, J. Chem. Soc. Chem. Commun., (1976) 919.

7 (a) K. Wade, J. Chem. Soc. Chem. Commun., (1971) 792; (b) K. Wade, Adv. Inorg. Chem. Radiochem., 18 (1976) 1.

8 D.M.P. Mingos, Nature (London) Phys Sci., 236 (1972) 99.

9 J.W. Lauher, J. Amer. Chem. Soc., 100 (1978) 5305.

10 J.S. Bradley, G.B. Ansell and E.W. Hill, J. Am. Chem. Soc., 101 (1979) 7418; J.S. Bradley, G.B. Ansell, M.E. Leonowicz, and E.W. Hill, ibid., 103 (1981) 4968.

11 See for example: (a) P. Brint, E.F. Healy, T.R. Spalding, and T. Whelan, J. Chem. Soc. Dalton Trans., (1981) 2515; (b) R.L. DeKock and C.P. Jasperse, Inorg. Chem., 22 (1983) 3843; (c) M.A. Cavanaugh, T.P. Fehlner, R. Stramel, M.E. O'Neill, and K. Wade, Polyhedron, 3 (1984) in press.

12 Note that for an "ideal" arachno-geometry α 109° and the C atom lies on the wing-tip axis (h 0 Å), Fig. 3. However this gives an unacceptable structure with B(wing)–C 1.23 Å and B(hinge)–C 1.24 Å. The geometry chosen is that closest to the ideal which is sterically acceptable: BC distances are still rather short (see experimental section).

13 R. Hoffmann, S.D. Wijeyesekera, and C.N. Wilker, Organometallics, 3 (1984) 962; S. Harris and J.S. Bradley, Organometallics, 3 (1984) 1086.

14 N.M. Kostic and R.F. Fenske, J. Am. Chem. Soc., 104 (1982) 3879.

15 Changes in populations of CH⁻ π-orbitals do not affect C–H bond strength since the H atom lies in a nodal plane.

16 M.B Hall, and R.F. Fenske, Inorg. Chem., 11 (1972) 768; M.B. Hall, Ph.D. Thesis, University of Wisconsin, Madison, WI, 1971; R.F. Fenske, Pure Appl. Chem. 27 (1971) 61.

17 E. Clementi, J. Chem. Phys. 40 (1964) 1944.